Hindawi
International Journal of Aerospace Engineering
Volume 2023, Article ID 9082587, 24 pages
https://doi.org/10.1155/2023/9082587

Research Article

Research on Forecasting of the Compressor Geometric Variable System Based on the MAE Model

Cunjiang Xia, Yuyou Zhan, Yan Tan, and Wenqing Wu

Civil Aviation Flight University of China, Guanghan 618300, China

Correspondence should be addressed to Yuyou Zhan; zyyskma@163.com

Received 14 December 2022; Revised 14 March 2023; Accepted 1 April 2023; Published 20 April 2023

Academic Editor: Tuo Han

Copyright © 2023 Cunjiang Xia et al. This is an open access article distributed under the Creative Commons Attribution License, which permits unrestricted use, distribution, and reproduction in any medium, provided the original work is properly cited.

The compressor geometric variable system is vital for aeroengines, as it affects their performance and design. To monitor the compressor geometric variable system states and detect anomalies in real time, a t-step forecasting method based on the MAE (masked autoencoders) model was proposed in this article. Unlike previous studies that used simulated or lab-generated data, we use actual flight data recorded by the aircraft data acquisition system to make our results more realistic. Through our experimental efforts, the feasibility of forecasting the compressor geometric variable system based on the MAE model is verified. That is not only the first application of transformer models with a masked pretraining mechanism in time series forecasts but also taking the lead in exploring the possibility of this key system forecast. We also test the generalizability of our method across different types of aeroengines. Finally, to make our theories more reasonable and convincing, experiments on different aeroengine states, including the transition state and the steady state, are carried out.

1. Introduction

In the field of civil aviation, one of the key drivers for the development of aeroengines is to comprehend and be proficient in the operational protocols of different systems. Enhancing the maintenance efficiency of aeroengines, ensuring their safety and airworthiness, and optimizing the key system functions are paramount for the improvement of aeroengines' design ability and for guaranteeing flight safety [1–5]. As the basic control system of the engine, the compressor geometric variable system has the responsibility of stabilizing the flow state of the gas path.

If the control of the airflow state of the compressor is unstable, stall phenomena will occur [6]. If this phenomenon persists, the compressor blades and aeroengine components will experience strong vibration, and the blades could end up breaking. Additionally, the exhaust temperature of the engine will rise, and the thrust may suddenly decrease. In severe cases, the aeroengine may be damaged or even destroyed. As a result, the compressor geometric variable system is crucial to the process of controlling the flow path. Therefore, researching the system's code of operation and potential developments could help airlines and non-OEMs (original equipment manufacturers) gain a thorough understanding of the essential components of aeroengines.

In this study, we will explore the feasibility of forecasting the compressor geometric variable system and attempt to assess the effectiveness of this approach in various types of aero engines. The variable stator vane (VSV) system and the variable bleed valve (VBV) system make up the compressor geometric variable system which is a key component of the entire engine gas path system. Figure 1 shows the general structure of aeroengines. In the compressor, the entering fluid will be pressurized by first accelerating it via the kinetic energy imparted in the rotors, and then diverging channels will slow the fluid down so that the kinetic energy could be converted into potential energy [7]. However, rotating stalls and surges will make the system unstable, which means the aircraft's airworthiness would be influenced by the unsecured status of the engine.

When the compressor speed is consistent, increasing the airflow of the compressor will increase the axial velocity of the airflow (c_a), and the attack angle (i) will decrease or even be negative. If the negative value is too large, the separation of the blade basin occurs, and a vortex zone forms in the blade basin. Although the vortex zone will not continue to

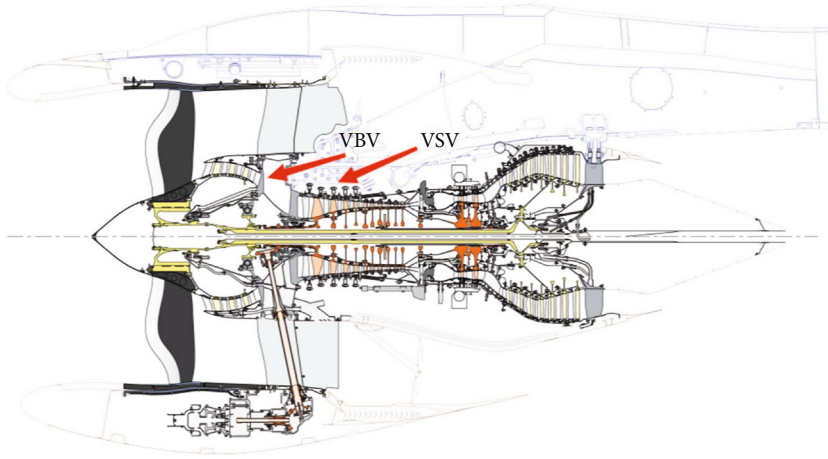

Figure 1: The general structure of aeroengines.

expand, the separation of the blade basin will reduce the operating efficiency of the blade and the flow capacity of the airflow at the section. Hence, the results will reduce the airflow at the compressor inlet and increase the degree of former-stage attack angles. In addition, decreasing the airflow of the compressor will decrease the axial velocity of airflow (c_a), and the attack angle (i) will increase. If the attack angle is too large, the airflow will separate from the back of the blade, which is known as the stall. With the compressor rotating, the stall area rotates in the same direction at a lower speed and gradually expands, which is called the rotating stall. Figure 2 presents these two kinds of burbling.

In order to avert the potentially dire consequences of burbling, the compressor geometric variable system will be highly instrumental in ensuring that this phenomenon is effectively taken care of in the compressor path. Furthermore, the VSV and VBV structures can modify the fluidic state by changing the angle of the VSV and the opening of the VBV, thus guaranteeing stable and efficient engine operation [8].

The introduction of artificial intelligence (AI) offers researchers the opportunity to model aeroengine systems and verify conjectures concerning the interaction of factors more quickly than was previously attainable due to the complexity of aeroengine studies. However, previous research on the compressor has not yet encompassed forecasting and modeling of relevant control systems; rather, it has been primarily devoted to fault diagnosis, fault prognosis, and flow forecasting. Castilho et al. presented an aircraft bleed valve fault classification method using machine learning methods [9]. Li et al. used a type of neural network to optimize the stator vane settings of multistage compressors [10]. Yan started research on fitting the operation curve of variable bleed valves [11]. Wang et al. presented an artificial immune algorithm to study the fault diagnosis of the variable bleed value system [12]. Cao et al. employed the least square support vector machine algorithm to investigate surge fault diagnosis [13]. Xuyun et al. utilized a type of neural network to forecast exhaust gas temperature [14]. Shuming et al. conducted a study on the fitting approach of the aeroengine baseline equation [15]. In addition to the references mentioned above, similar research is primarily conducted in relation to the aforementioned aspects. However, these analyses of aeroengine compressors have certain drawbacks.

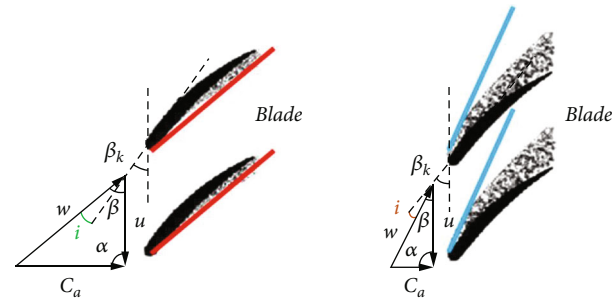

i: Attack angle
C_a: The axial velocity of airflow
u: Tangential speed of blade rotation
β: Angle of airflow inlet into the blade
β_k: Geometric inlet angle of the blade

Figure 2: The phenomenon of burbling.

(1) Datasets. Most of the data used in current compressor system research is sourced from open datasets, software simulations, or laboratory simulations, which puts limitations on their ability to accurately reflect the actual conditions of aeroengines. On the contrary, datasets that are collected during actual flying conditions are more effective in providing a more accurate representation of aeroengines

(2) Limited parameters. Due to the complexity of **an** aeroengine, it is indispensable to take into account all the relevant elements that can affect the compressor. The studies aforementioned have only focused on VSV or VBV parameters, neglecting other aspects **and** leading to incomplete conclusions

(3) The applicability of the experimental conclusion is questionable due to the lack of a control experiment.

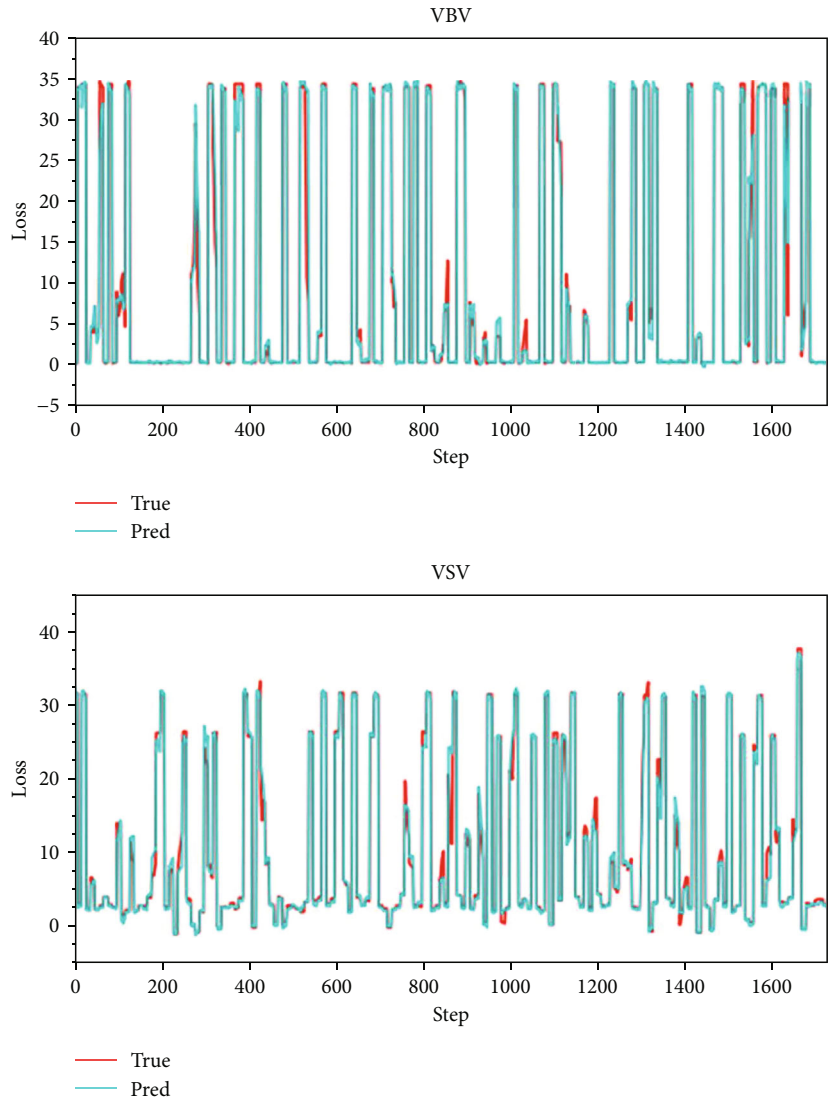

Figure 3: The result forecasted by masked autoencoder (MAE) model based on type B aeroengines.

Table 1: Parameter selection (A).

Parameter	Unit
Ambient pressure (P0)	PSIA
High-pressure compressor outlet pressure (PS3)	PSIA
Throttle lever angle (TRL)	°
Fan inlet temperature (T12)	°C
High-pressure compressor inlet temperature (T25)	°C
Total air temperature (TAT)	°C
Low-pressure rotor speed (N1)	%RPM
High-pressure rotor speed (N2)	%RPM
Variable stator vane (VSV)	°
Variable bleed valve (VBV)	°

Table 2: Parameter selection (B).

Parameter	Unit
Altitude	Feet
Throttle lever angle (TRL)	°
High-pressure compressor inlet temperature (T25)	°C
High-pressure compressor outlet temperature (T3)	°C
Total air temperature (TAT)	°C
High-pressure compressor outlet pressure (PS3)	PSIA
Low-pressure rotor speed (N1)	%RPM
High-pressure rotor speed (N2)	%RPM
Variable stator vane (VSV)	°
Variable bleed valve (VBV)	°

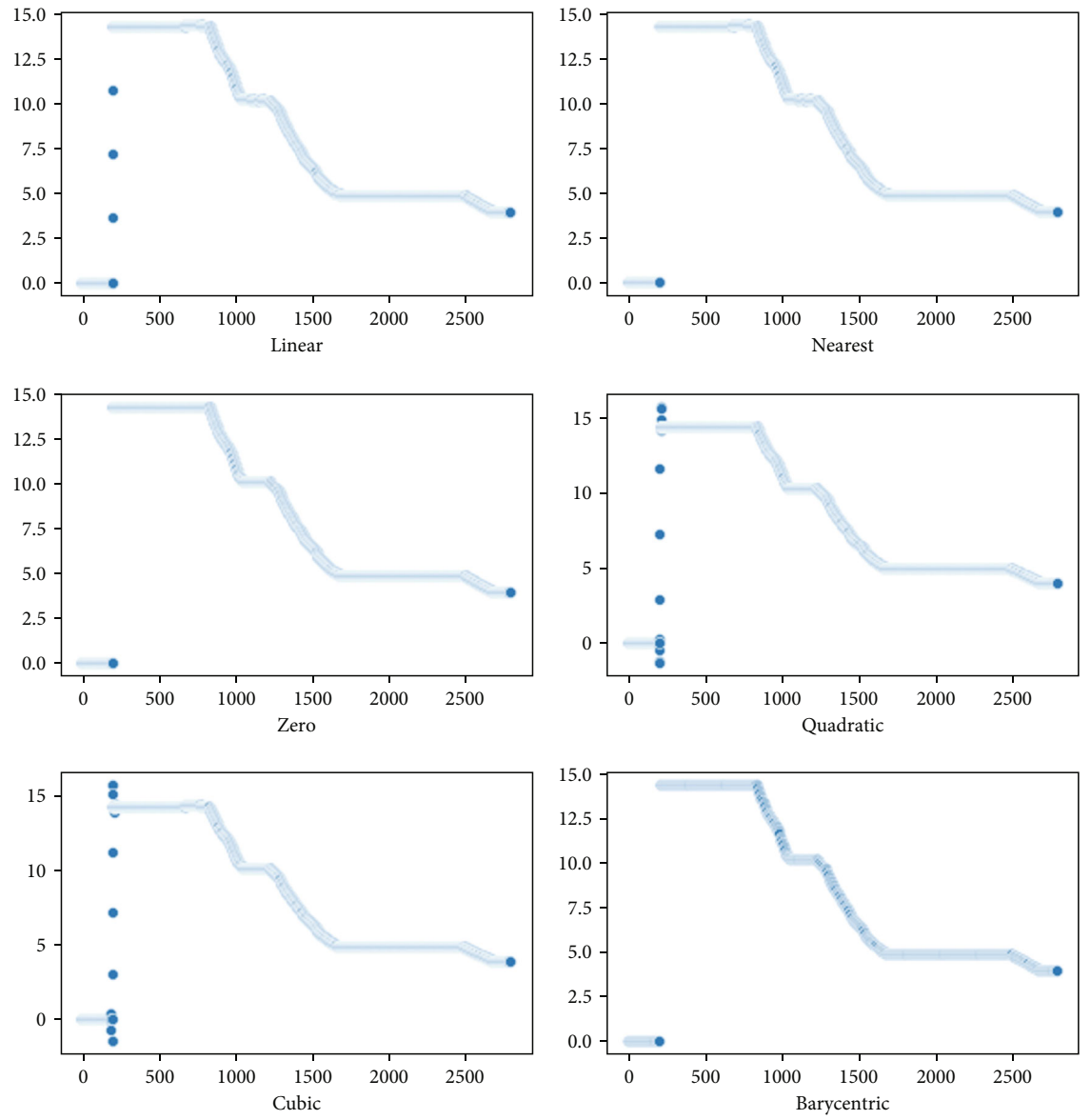

Figure 4: Comparison results of interpolation methods.

The effectiveness of other aeroengine types must also be taken into account in order to make the outcome more reliable and applicable

(4) The study of forecasts is always lacking, which is an important part. The description of the forecasting method remains unclear. Analyzing fault diagnosis and failure prognosis is a pressing issue; however, it falls under the realm of fault detection. If the compressor geometric variable system can be forecasted, **an** early fault detection requirement may be satisfied, while also aiding in the analysis of the underlying principles behind the entire compressor system

In this article, a new methodology based on masked autoencoders (MAE) and multiparameter fusion is proposed for forecasting the aerodynamic-engine compressor geometric variable system. To create the datasets for this research, data from aircraft data-gathering systems were utilized. By comparing the abovementioned related research and the various questions raised, our paper's novelty and contribution are as follows:

(i) This paper is the pioneering effort to analyze the feasibility of predicting the geometric variables of an aeroengine compressor system and to suggest a highly precise method. Additionally, the method has been extended to different types and varying conditions of aeroengines, illustrating its robustness to an appreciable degree

(ii) The data for this study was sourced from aircraft data acquisition systems. In comparison to the open-source datasets that are typically utilized by other researches, real flight data can more accurately reflect actual compressor operation status. This promotes

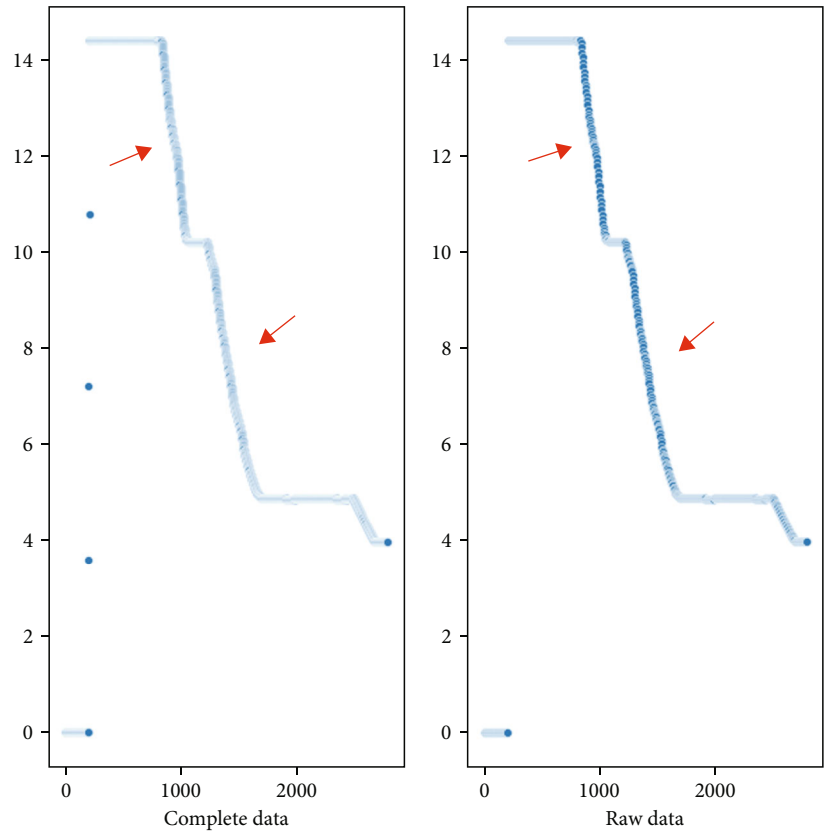

Figure 5: Comparison results of complete data and missing data.

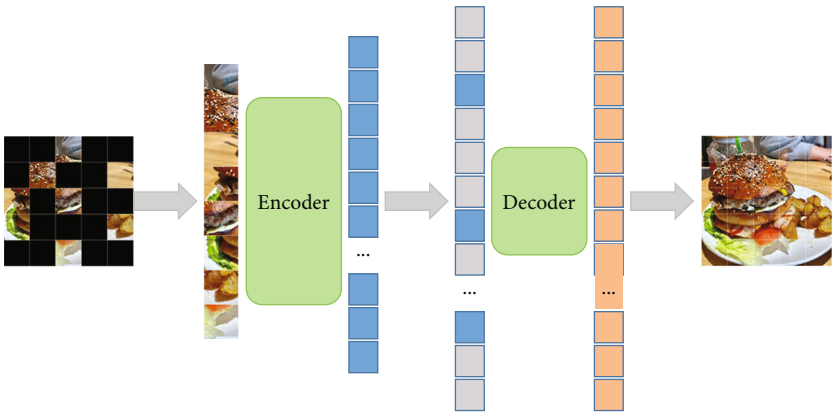

Figure 6: Original MAE architecture.

the accuracy of the AI model's predictive results and brings them closer to the desired outcome

(iii) This article leverages the MAE model to address a time series problem. Not only is this an example of the straightforward application of MAE in the field of time series but it also proves the usefulness of the model for multitarget prediction tasks by performing pretraining tasks aided by the masked mechanism, which is conducive to the exchange of advanced technologies across various disciplines for the purpose of addressing important issues.

Figure 3 displays parts of the outcomes anticipated by the MAE model.

The forecasted results of the masked autoencoders (MAE) model, displayed in the above image as changes in VBV opening (unit: °) and VSV angle (unit: °), are based on type B aeroengines.

2. Data Preprocessing

2.1. Data Source. Previous relevant studies mainly made use of simulation data, open-source datasets, datasets generated

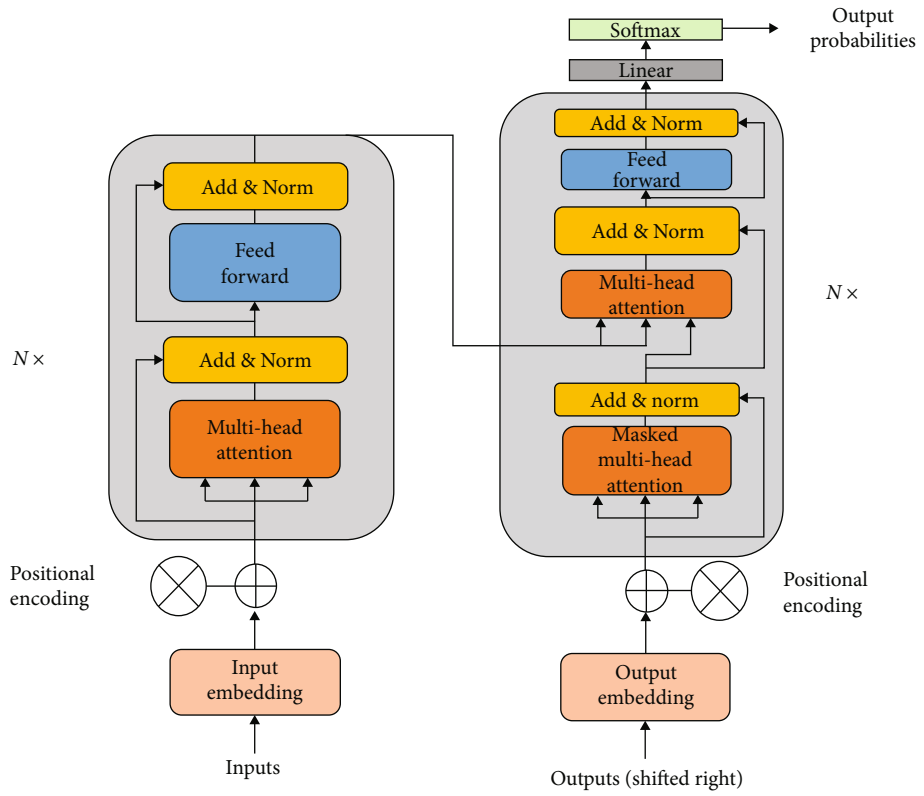

Figure 7: The transformer-model architecture.

from labs, and aircraft data acquisition systems. In this article, we utilized datasets from the aircraft data acquisition system data which were recorded during the actual flight, providing us with more precise information than traditional methods. Specifically, these systems are designed to collect various critical parameters of planes in real-time, enabling a more accurate assessment of the compressor's operational state. In addition to various and detailed parameters, continuous storage, easy export, and the ability to process data [16], our datasets also have the crucial advantage of increasing the validity and thoroughness of our research. It is important to note that the type of aeroengine we focused on was the dual-rotor turbofan engine; thus, the datasets specifically pertain to this type of engine and cannot be applied to others.

In addition, the operation conditions of an aeroengine are typically divided into a transition state and a steady state, which always run through each complete flight. Thus, the aircraft data acquisition system records not only the entire flight process but also the state changes in the aeroengine throughout it. To enable the model to recognize the current aeroengine states based on the input data, random data samples are extracted and fed into the model. At this time, both steady state and transition state data are randomly chosen so as to provide the model with the necessary input. With enough complexity, the model can learn the patterns of these two states during training and identify the current state based on the input data during the prediction process. This type of random data extraction training model grants the model universality and eliminates the need for separate

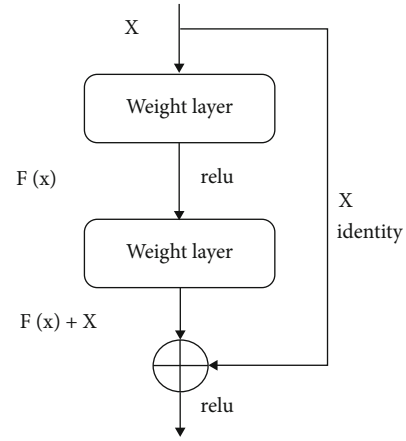

Figure 8: Residual learning: a building block.

modeling. To prove the feasibility of predicting these two aeroengine states as well as the possibility of general models, this paper will discuss them as part of the experiment in Part 4.2.3.

2.2. Parameter Selection. Our goal with this work is to accurately forecast the variation of VSV and VBV. Accordingly, the angle of VSV as well as the opening of VBV are used as target values. It is important to note that in this article, situations wherein time series data is utilized are referred to as "steps." In the present research, the step is defined as the frequency of recording data. One step can be representative of

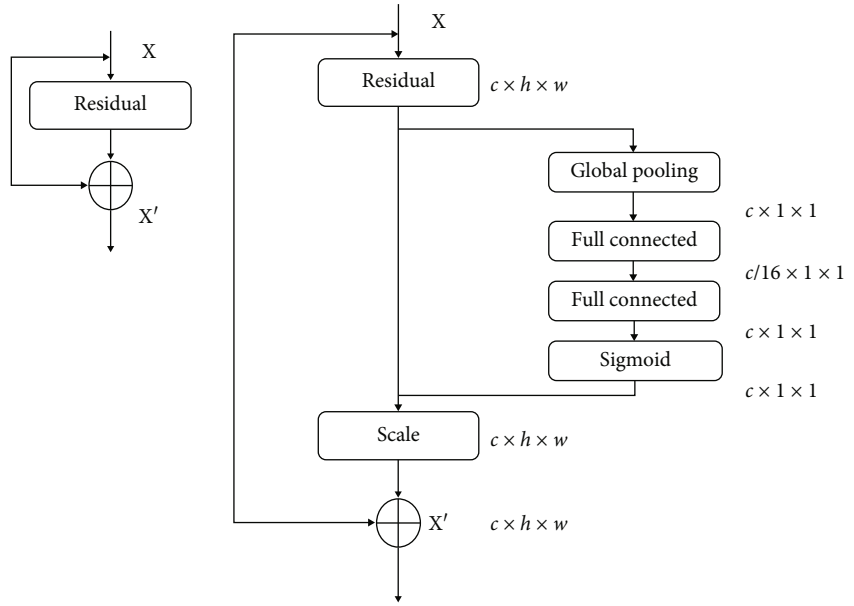

Figure 9: SE-ResNet module.

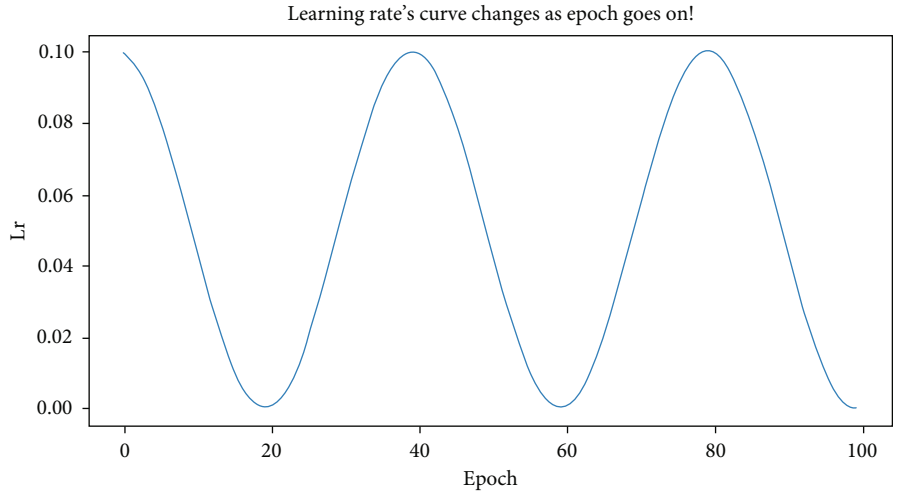

Figure 10: Cosine annealing LR (T max = 25).

the sensor acquisition rate which is 1 Hz in our study. To forecast 10 in the future, we primarily use correlative parameters in 100 steps. And the reason for utilizing these step settings is that applying the MAE model to longer input timespans allows it to more accurately recognize the state and changes within the input data, thus making forecasting more accurate.

In the process of parameter selection, the interaction of factors, previous relevant research settings, and based on the technology of aeroengines as well as the capability of data acquisition [17, 18] should be considered in order to provide better forecasting and tracking of changing trends in key structures and guarantee the stable and safe operation of the superior system, thereby ensuring the airworthiness of aircraft. The following parameters of type A aeroengines in Table 1 will be selected.

Table 3: Parameters of cosine annealing LR.

Parameter	Meaning
$\eta^i_{\min}$	Minimum learning rate
$\eta^i_{\max}$	Maximum learning rate
T_{cur}	Current epoch
T_i	Number of periods

Different types of aeroengines have different aircraft data acquisition systems; thus, the parameters that can be collected vary slightly depending on the type of aeroengine. In order to reduce the interference of extraneous variables, we

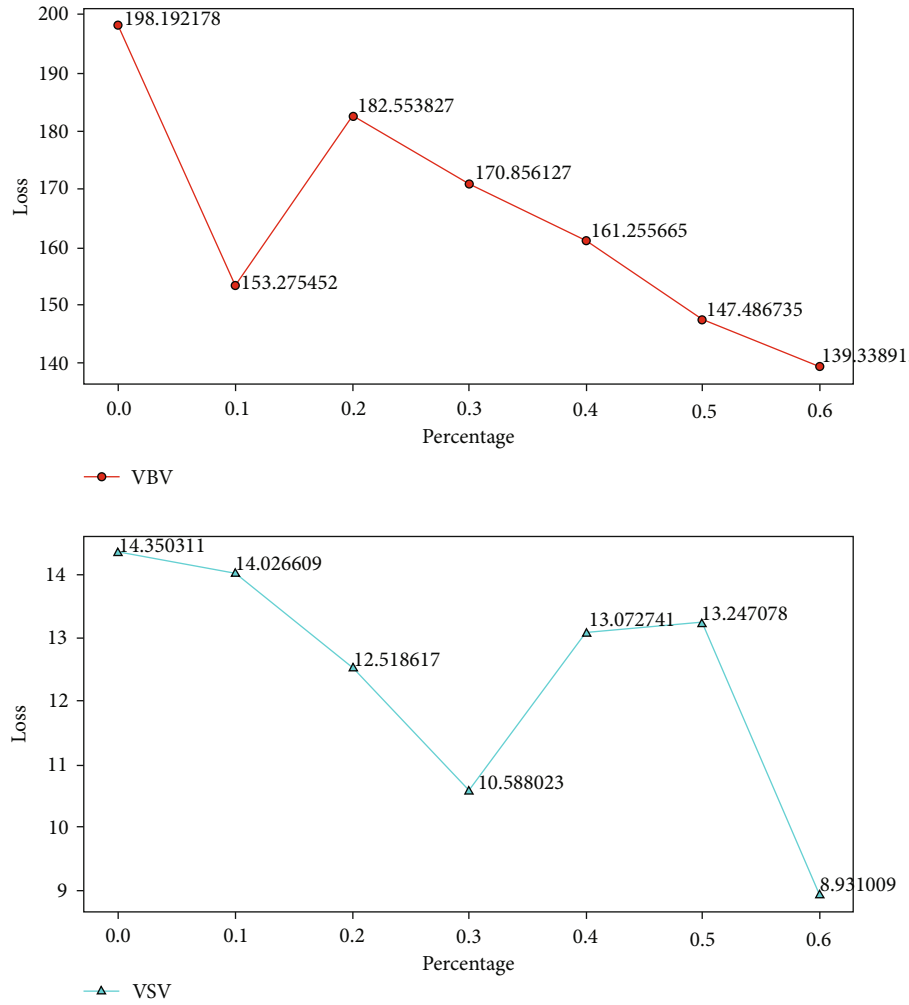

Figure 11: The result of different pretraining data percentages (type A aeroengine).

endeavor to maintain the selection of essential parameters for type B aeroengine in Table 2.

In addition, the input values will be the randomly sampled continuous 100 steps as one batch, and the output will directly be the VSV or VBV values (°) in the next 10 steps. The 100-step data might include enough and essential latent future information to predict what we need.

2.3. Interpolation of Missing Data. In this paper, we compared the different interpolation methods such as linear, nearest, zero, quadratic, cubic, and barycentric. Figure 4 shows the results of the above interpolation methods using the P0 factor in one flight. It is apparent from this figure that each method does not affect the general trend, but the linear is smoother and has no outlier data. Consequently, the linear will be a good concern relatively. Figure 5 presents the comparison of complete data and raw data using the P0 factor in one flight.

2.4. Random Sampling. Using a random sample strategy, a more general and accurate model will be built. This method can improve how well our model matches the actual latent control function. Because we hope that our model can predict factors' changing and interaction instead of learning the temporal relationship of flight segments [19, 20], one batch consists of 100 continuous steps as input values and 10 uninterrupted steps as output values. In the experiment section, we will randomly sample 64 batches as the input to a round of training. And Part 4.2.3 will present the strategy's accurate outcome.

3. Method

To explore whether the features of the algorithm itself could, in certain cases, increase the accuracy of forecasting target values. To that end, some classic and advanced learning algorithms have been utilized in this study for comparison. But it is not the focus of our work. This study explores the feasibility of forecasting the compressor geometric variable system using the MAE model, a cutting-edge deep learning algorithm that is fresh to the field of computer vision (CV).

3.1. Masked Autoencoders. This state-of-the-art computer vision (CV) algorithm was proposed by He et al. [21] in 2021. This model is the application of a transformer [22] in CV, and it uses the mask mechanism in pretraining,

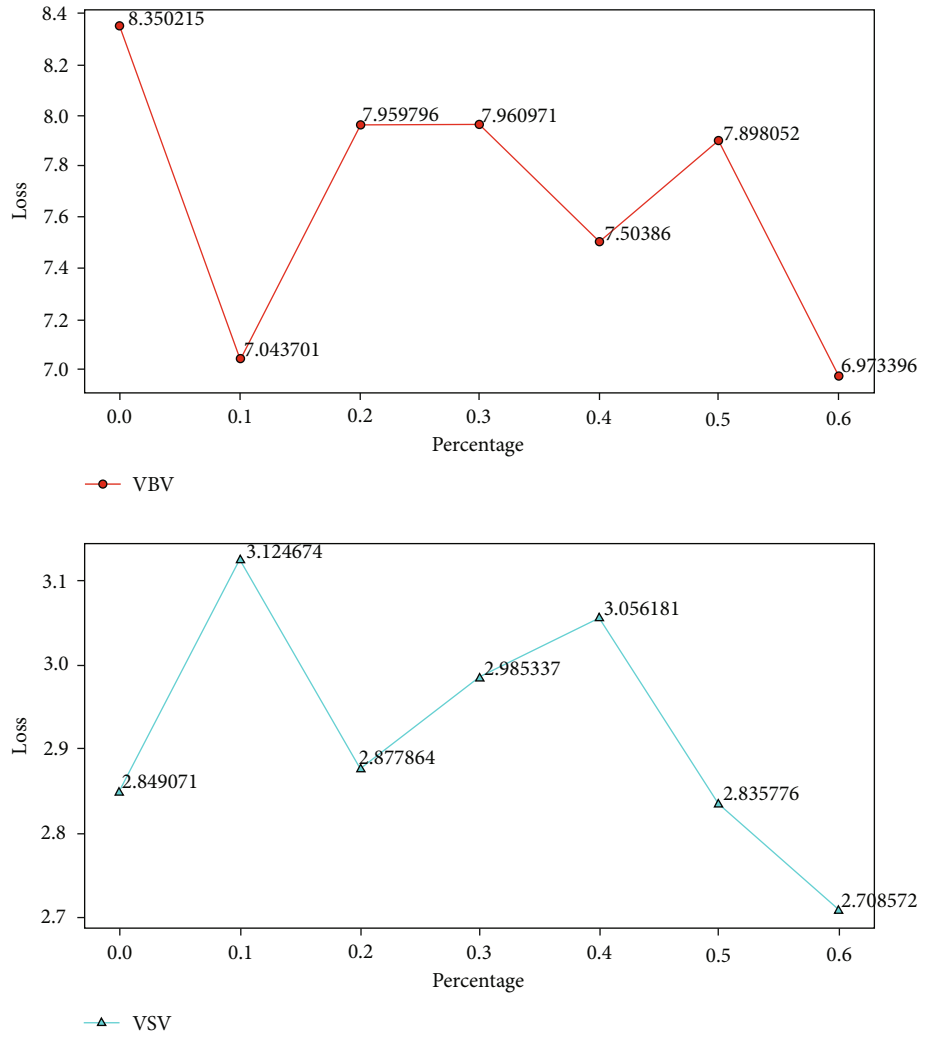

Figure 12: The result of different pretraining data percentages (type B aeroengine).

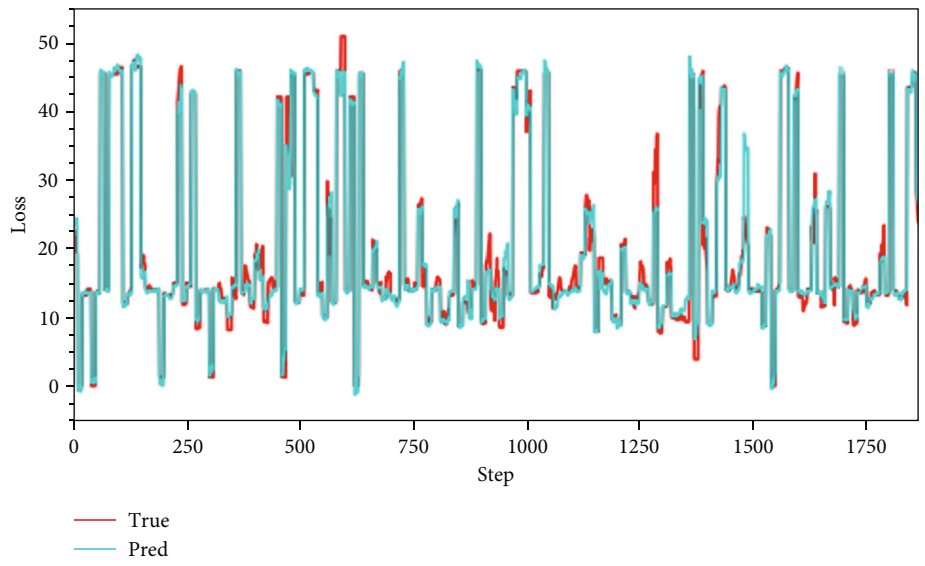

Figure 13: The entire forecast result of VSV angles (type A aeroengine).

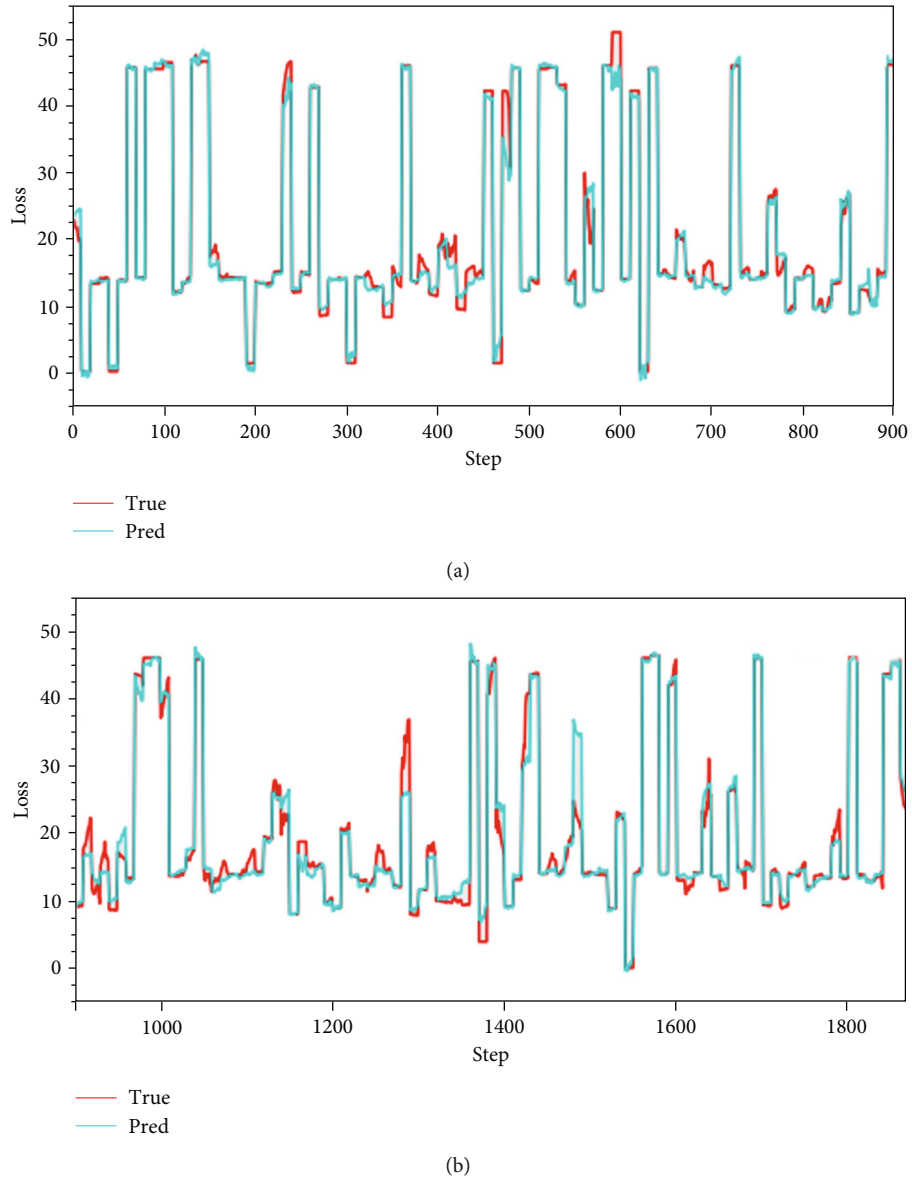

Figure 14: (a, b) The partial forecast result of VSV angles (type A aeroengine).

which is similar to BERT [23]. Figure 6 shows the entire idea of this architecture. It is simple but powerful. The model could further learn latent representation among parameters by reconstructing the original image that was randomly masked for 75% of the area in the pretraining task; hence, a difficult task is created that cannot be easily solved by extrapolation from visible neighboring areas (see Figure 6). Then, the highly sparse input creates an opportunity for designing a powerful encoder.

Inspired by this idea, pretraining could enhance the learning of the global relationship between parameters, and adding positional embeddings could mean that the latent temporal information would be learned.

The traditional recurrent neural network (RNN) transmits information in time sequence, but it cannot have good parallelism. Although the convolutional neural network (CNN) may produce multichannel output to learn important features, it is difficult to merge remote data. The transformer uses multihead attention to simulate multichannel, hopefully learning the key features we want. The RNN uses the output from the last step to transmit it to the next step for input. In contrast, the transformer directly grabs the information throughout the sequence through the attention layer for aggregation. Therefore, the attention layer already has the features that I need. As a result, the model only needs to focus on how to effectively capture the sequence information that we need. The structure of the transformer is shown in Figure 7. To meet our research aim, we have lightly modified these models to better match our research. We changed the size of the kernel, stride, and padding so that we could directly input datasets into the models. In addition, we added one or two linear layers at the rear of the models. Thanks to the above methods, we cannot only adapt the model to the dimensions of the dataset perfectly

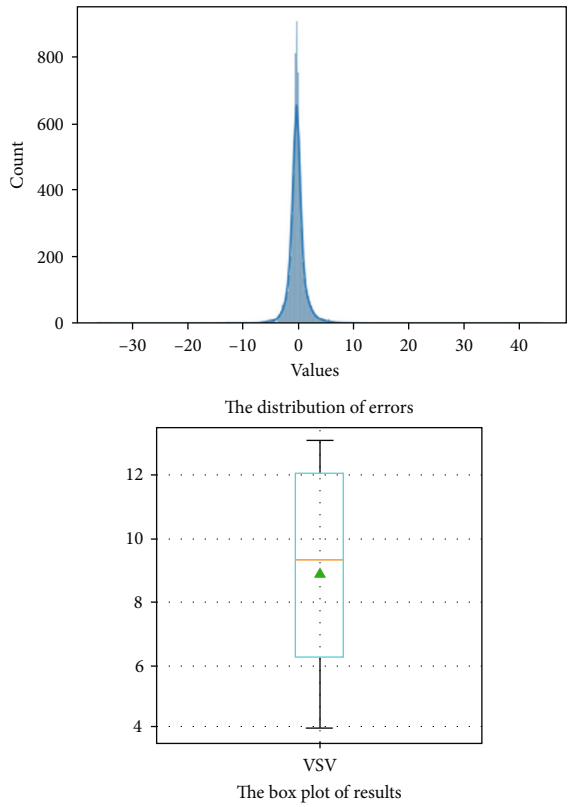

Figure 15: The distribution of errors and the box plot of results (VSV, type A aeroengine).

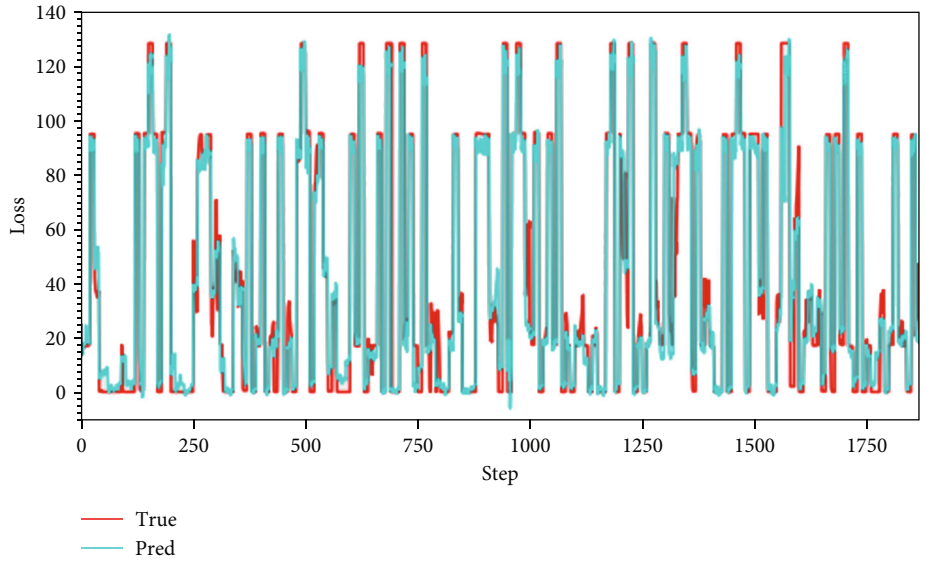

Figure 16: The entire forecast result of VBV opening (type A aeroengine).

but also better fit the prediction results through the linear layer.

3.2. Residual Network. According to experience, the deeper the network is in the field of deep learning, the better it is able to extract more complicated features. However, further

Table 4: Comparison of models' test loss.

Model	Loss (MSE)
SENet18	5.098
MAE	8.931
ResNet18	9.024

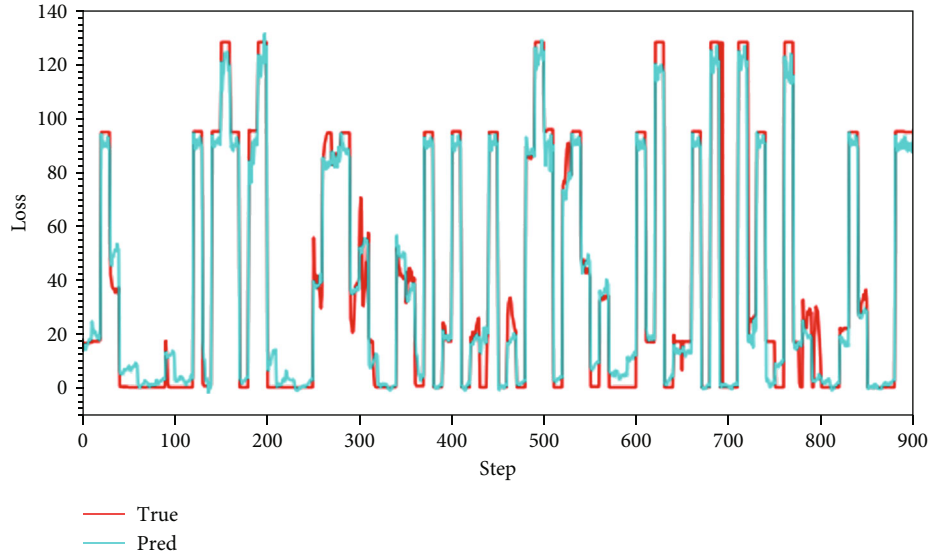

(a)

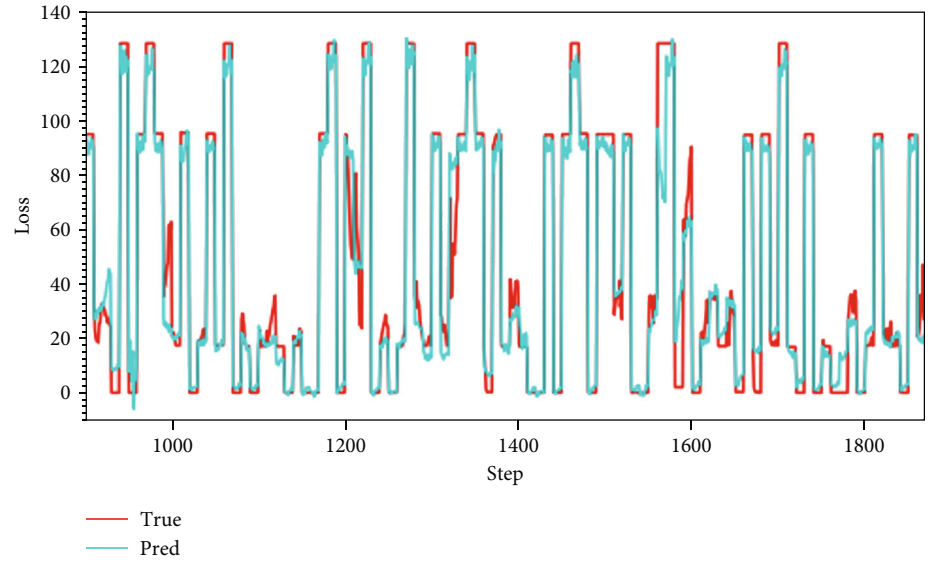

(b)

Figure 17: (a, b) The partial forecast result of VBV opening (type A aeroengine).

research reveals that despite the network depth increases, the model presents a degradation phenomenon, which indicates that as the grid's depth rises, the accuracy of the network saturates or even declines. But this problem is not caused by overfitting, because adding extra layers to the appropriate model will result in larger training errors [24, 25]. In an ideal environment, the result of deeper network training will be no worse than that of the shallow network. If the previous shallow network has done the training work, the latter deep network only needs to be used for identity mapping, which means the input X is equal to the output X. It is equivalent to learning the weight as $1/n$ so that the input is equal to the output. Unfortunately, in practice, it turns out that the optimum theoretical solution cannot be found by stochastic gradient descent (SGD). Based on the above problems, the residual network proposes a deep residual learning framework and constructs an identity mapping to solve the degradation problem when the network depth increases. If the expectation function is expressed as $H(x)$ and the learned result is X, the next layer network does not learn a new x as before but learns the residual $f(x)$ between $H(x)$ and X. Therefore, the output of the next layer is the sum of the shortcut connections of the $f(x)$ and the X. And the technique will not increase the computational complexity. The framework of residual networks is presented in Figure 8.

3.3. Squeeze-and-Excitation Network. SENet starts from the feature channel, models the relationship between the feature channels through two operations: sequence and exception, and automatically obtains the importance of each feature channel, which means the weight, through learning. Then, depending on the weight learned, we could improve the

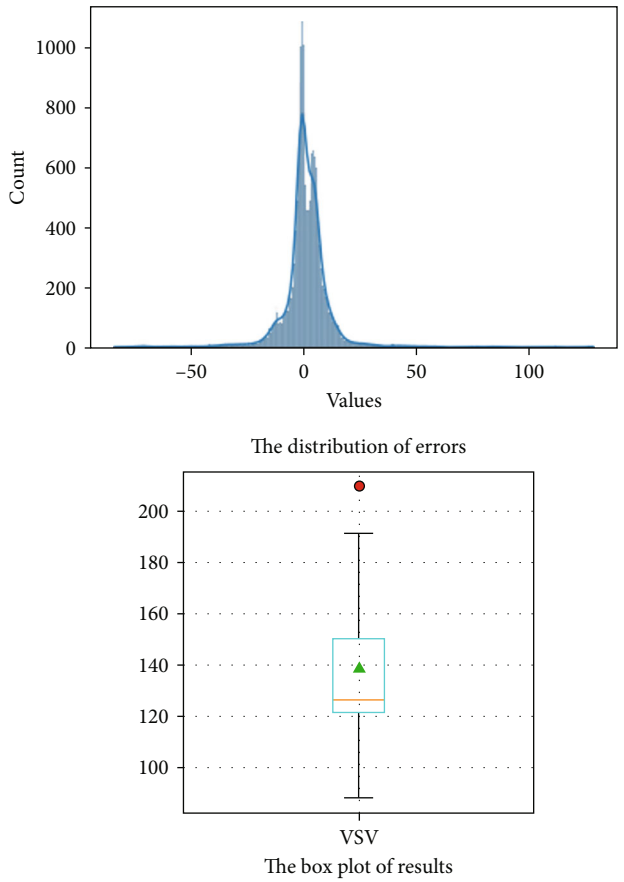

Figure 18: The distribution of errors and the box plot of results (VBV, type A aeroengine).

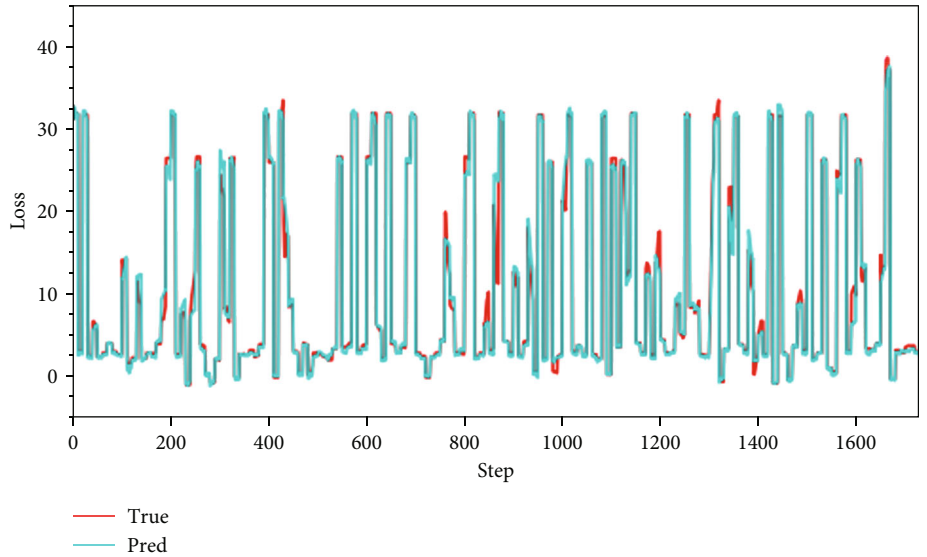

Figure 19: The entire forecast result of VSV opening (type B aeroengine).

useful features and suppress the features that are not useful for the current task.

The squeeze operation compresses features along the spatial dimension and converts each binary feature channel into a real number. Here, global average pooling is used as the squeeze operation. In this way, the real number has a global receptive field to some extent, and the output dimension matches the number of inputs in the feature channels,

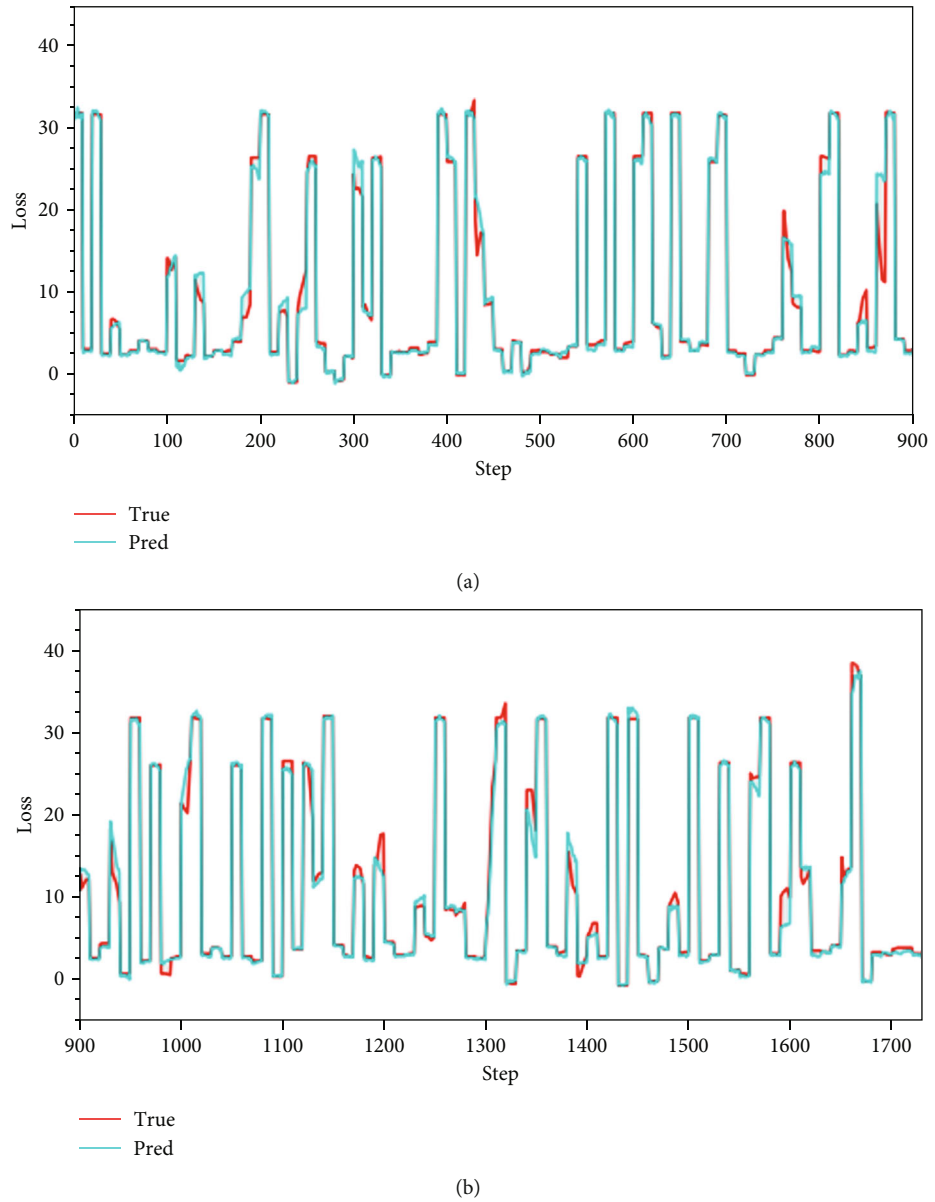

Figure 20: (a, b) The partial forecast result of VSV opening (type B aeroengine).

which represents the global distribution of response on the feature channels and enables the layer close to the input to obtain the global receptive field.

$$F_{sq}(u_c) = \frac{1}{H \times W} \sum_{i=1}^{H} \sum_{j=1}^{W} u_c(i, j), z \in R^C. \quad (1)$$

The exception operation builds the correlation between channels across two full connection layers and produces the same number of weights as the input features.

$$F_{ex}(z, W) = \sigma(W_2 \text{ Re LU}(W_1 z)), \quad W_1 \in R^{C/r \times C}, W_2 \in R^{C \times C/r}. \quad (2)$$

The entire operation can be seen as the learning of the weight coefficients of each channel through the SE block and a weighting of each channel item by item through scale. In this way, we could make the model more capable of identifying the features of each channel. It is the application of the attention mechanism to channels. Therefore, the features in each channel that have an important impact on the model can be extracted through the SE module. Figure 9 shows the framework of the SE block.

4. Prediction Experiments

In our experiment section, the feasibility of prediction must be tested and the applicability of forecasting verified. It should be noted that the datasets we used in this paper are neither standardized nor normalized; the angle (°) of VSV

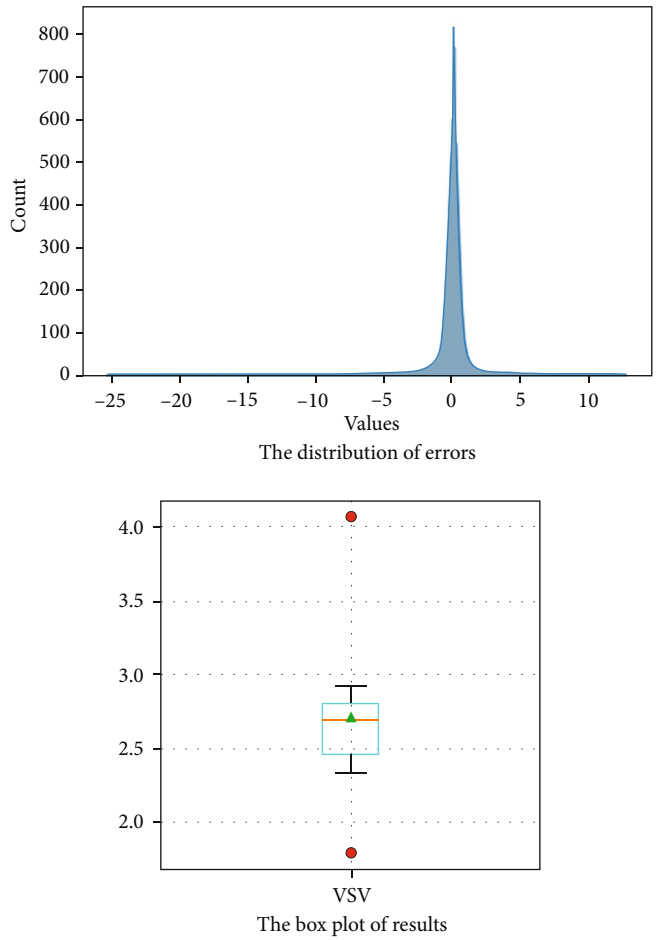

Figure 21: The distribution of errors and the box plot of results (VSV, type B aeroengine).

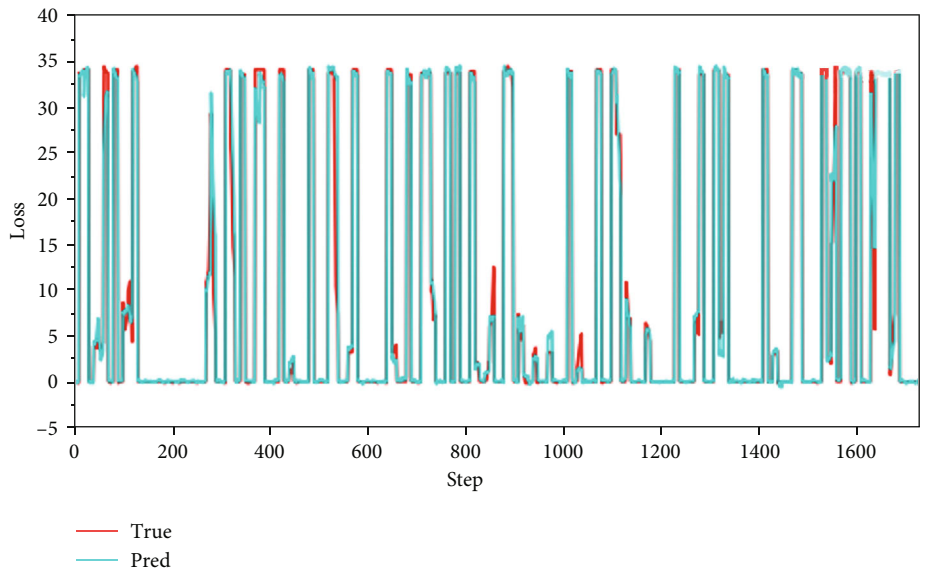

Figure 22: The entire forecast result of VBV opening (type B aeroengine).

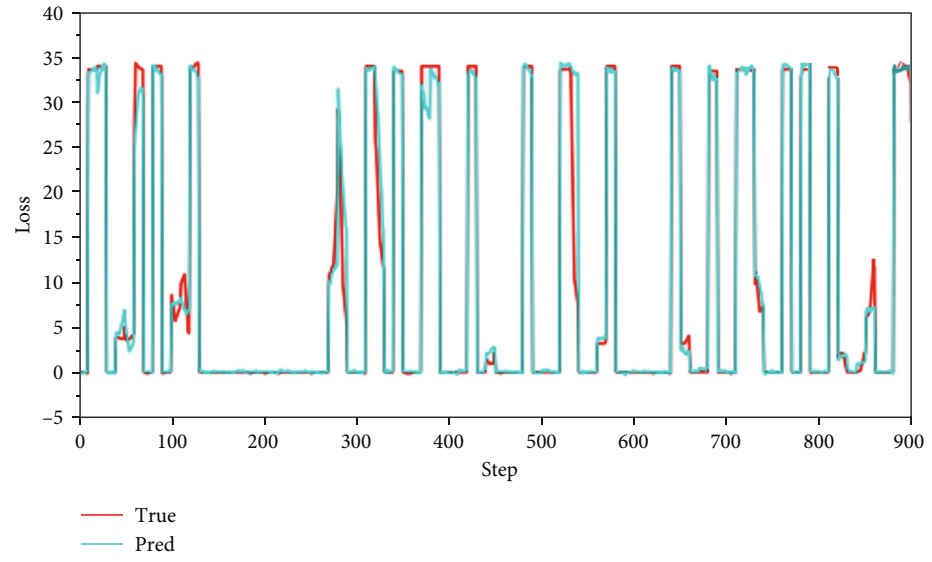

(a)

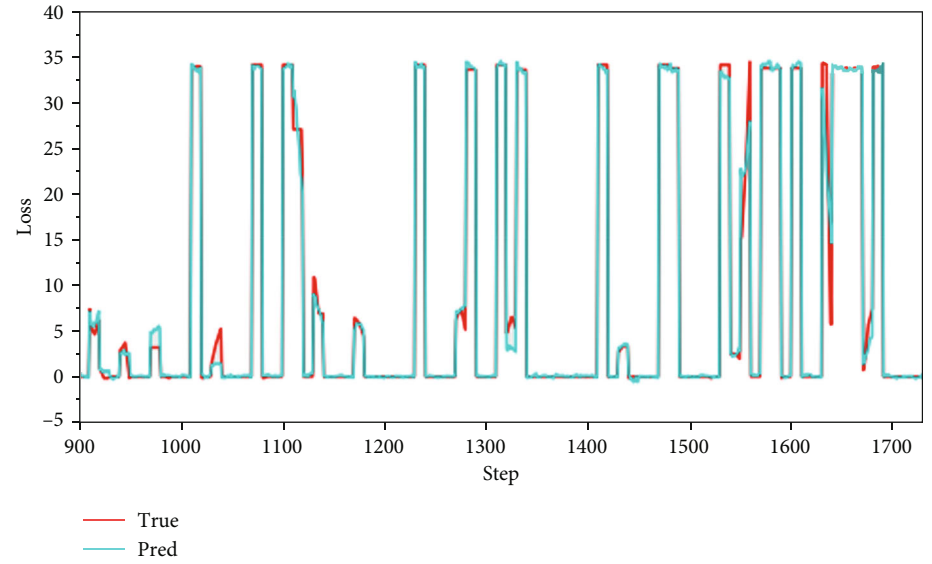

(b)

Figure 23: (a, b) The partial forecast result of VBV opening (type B aeroengine).

and the opening (°) of VBV can be directly reflected in the output. And the mean square error (MSE) will be used to measure the performance of our results. Therefore, the result of MSE is the square of the angle (°) and the opening (°). Finally, the x-axis step in the following figure represents the change over time.

$$\frac{1}{m}\sum_{i=1}^{m}\left(y_i - \widehat{y}_i\right)^2 \tag{3}$$

Meanwhile, all MSEs are yielded by the mean error of ten different offset experiments which use the minimum test error model. And the different offsets will make the data input to be different. But all input data comes from the same test datasets and has only the offset. And the offset will make the extracted data different every time. It should be noted that the unit of VSV and VBV systems predicted in this paper is the degree (°), so the numerical result forecasted in subsequent experiments is the square of this unit, while the y-axis of the trend chart is this unit. And the gray area between different curves is the loss (the difference between the true and the forecasted). Our experiment simulates a real situation, where the model receives the data collected by the aircraft data acquisition system and makes predictions. Therefore, the difference between the data-generation environment and our experiment is small. This method is similar to testing the model by inputting the test set and getting the output of the model.

4.1. Hyperparameter Setting. The optimizer we used is adaptive moment estimation with decoupled weight decay

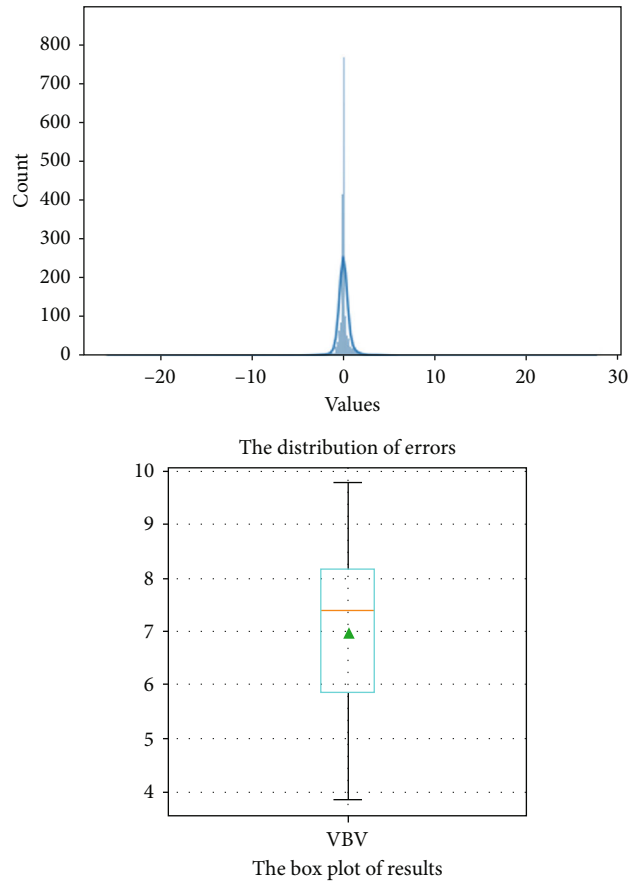

Figure 24: The distribution of errors and the box plot of results (VBV, type B aeroengine).

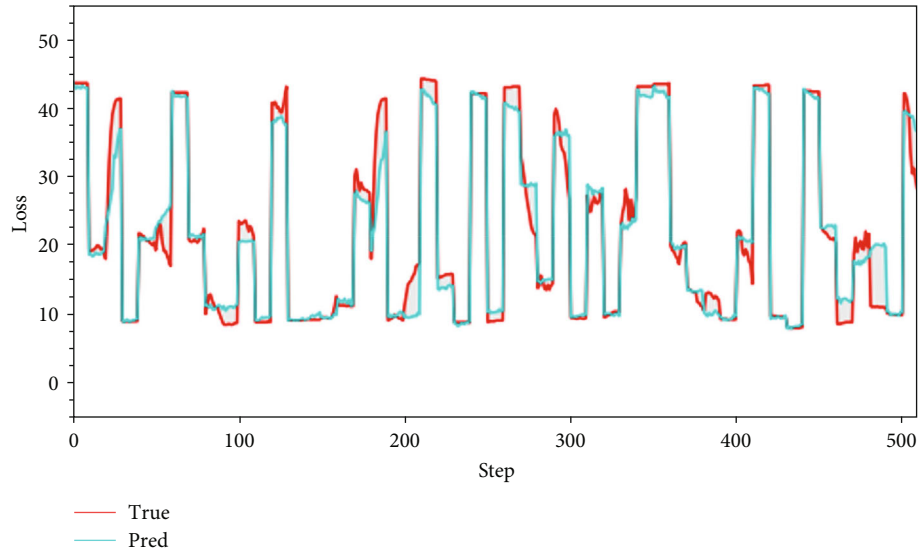

Figure 25: The transition state (VSV, type A aeroengine).

(AdamW). And the setting of hyperparameters will be presented later [26]. Hyperparameters $\beta_1 = 0.9$, $\beta_2 = 0.95$, and weight_decay = 0.05 during pretraining. And we employ $\beta_1 = 0.9$, $\beta_2 = 0.999$, and weight_decay = 0.05 during downstream tasks. In order to control the learning rate and prevent wandering near the optimal solution, we adopt a cosine annealing learning rate. And according to Formula (4), we could show the variation in general trends of learning

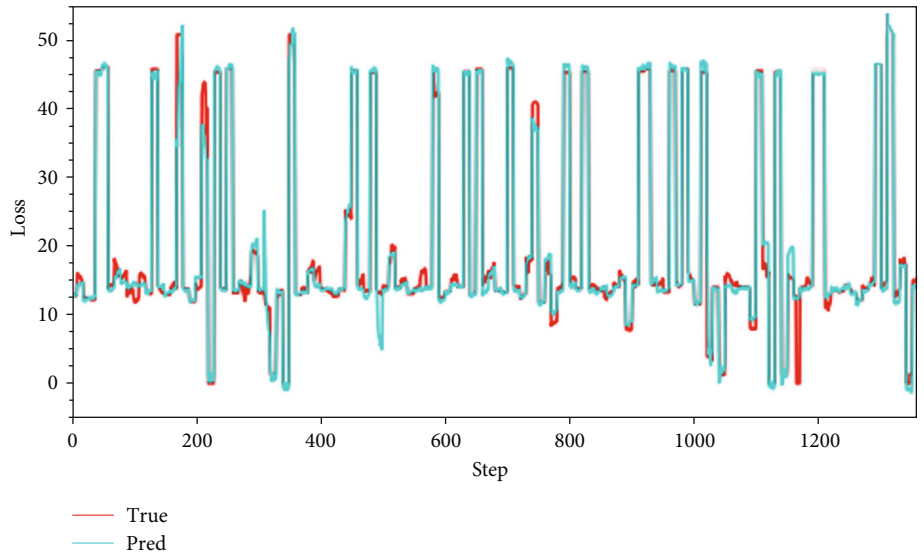

Figure 26: The steady state (VSV, type A aeroengine).

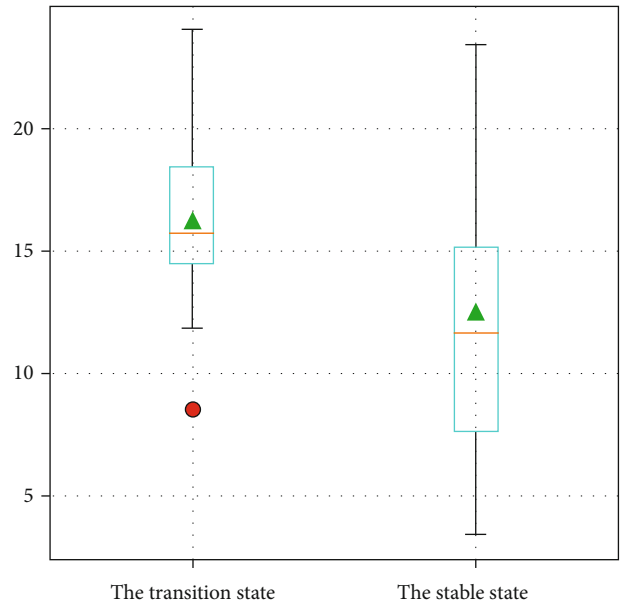

Figure 27: The box plot of the two states (VSV, type A aeroengine).

rate when we are training models (see Figure 10). The meaning of these parameters will be presented in Table 3.

$$\eta_{\mathrm{lr}} = \eta_{\min}^{i} + 0.5 \times \left(\eta_{\max}^{i} - \eta_{\min}^{i}\right) \times \left(1 + \left(\cos \frac{T_{\mathrm{cur}}}{T_i}\pi\right)\right). \quad (4)$$

In order to divide the proportion of pretraining datasets, we carried out some experiments. Figures 11 and 12 show the results. The results show that for the two types of aeroengines to produce the optimum outcomes, 60% pretraining data is required. And we chose not to increase the proportion of pretraining data in order to avoid affecting the formal training process. In addition, it is obvious that directly training the MAE model cannot reach the minimum error; hence, the pretraining task is necessary.

4.2. Result Analysis

4.2.1. Feasibility Analysis. Figure 3 presents the changes in VSV angle and VBV opening forecasted by the MAE model in type B aeroengines. But the type A aeroengine is considered as our study objective during the initial stage of our research. To explore the feasibility of forecasting the compressor geometric variable system, we carried out some key experiments on the type A aeroengine. Figures 13–16 show the details of the VSV angle prediction results. The difference between the real value line and the predicted value line is clearly shown in these figures. Whether in

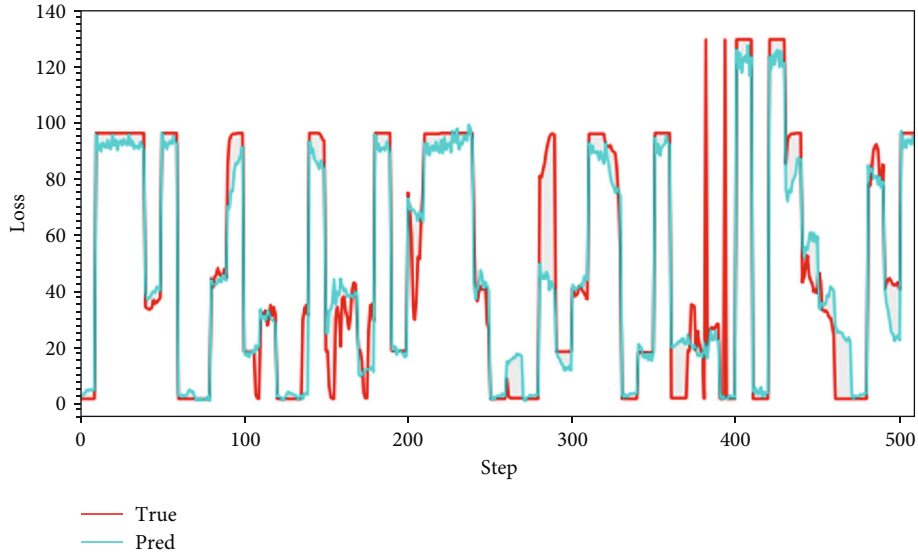

Figure 28: The transition state (VBV, type A aeroengine).

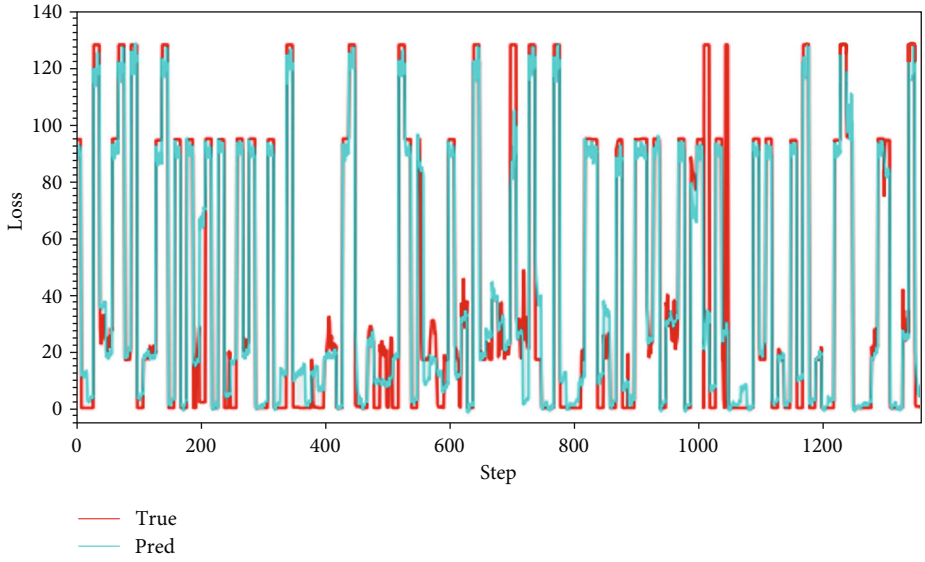

Figure 29: The steady state (VBV, type A aeroengine).

whole or in part, the error is low, and the overall trend of the forecast is consistent with the real value line. And the average value of test experiments is 8.931 (the square value of angles °). It is clear that the forecast result is acceptable. The comparison results of different models are presented in Table 4. It should be noted that the triangle in all box plots represents the position of the average value. Circles represent outliers.

The MAE model obtains a good score but is inferior to the SENet18 model. According to the structures of the two models, the reason why the MAE model cannot achieve the best could be that the MAE model is an extremely complex model, which means that in addition to its own powerful pretraining mechanism, it also needs more data to complete learning tasks. And the SENet18 is a light learning model, which means that with the same data scale, it might train the model faster [21, 27]. This is the reason why the SENet18 performs better. Therefore, in future research, the datasets need to be expanded.

In addition, Figures 16–18 present the details of the VBV opening prediction results. The average value of test experiments is 139.339 (the square value of angles °). The figures below show that the forecast errors of VBV openings are larger than those of VSV angles. And 139.339 is a big number, but the results of the forecast in these pictures are still acceptable. It can be seen that the VBV opening is a wide range of changes, which is the reason why the value of this error is gone great at the numerical level, but the forecasting effect is still relatively accurate. The MAE model can still track the change in VBV openings immediately and

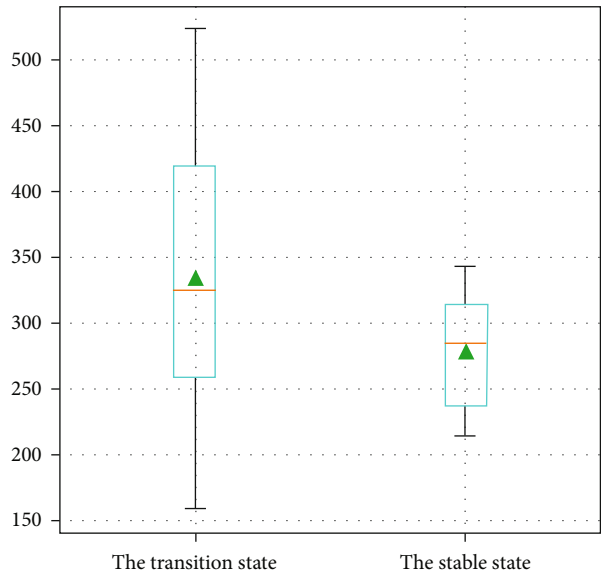

Figure 30: The box plot of the two states (VBV, type A aeroengine).

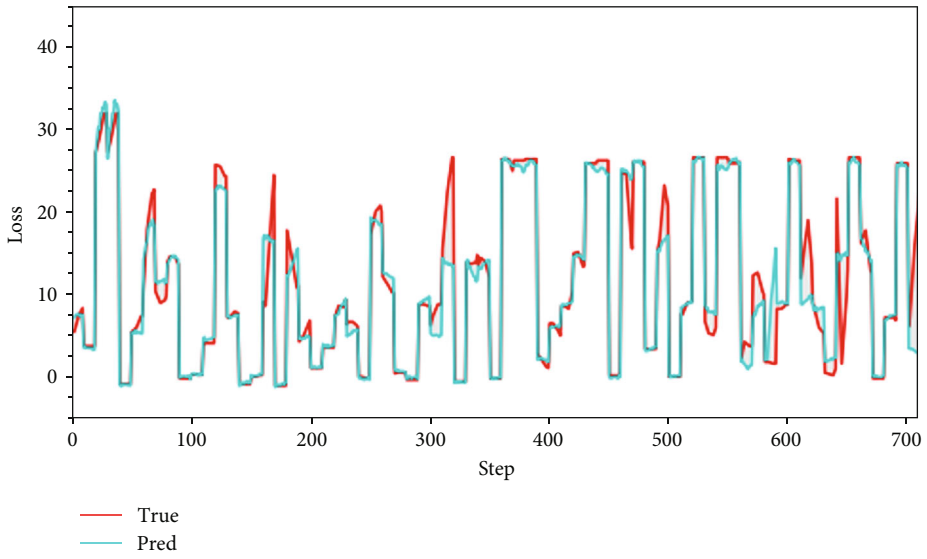

Figure 31: The transition state (VSV, type B aeroengine).

effectively. Therefore, the feasibility of forecasting the compressor geometric variable system is verified.

4.2.2. Applicability Analysis. Part 4.2.1 shows the proof of the feasibility of forecasting the compressor geometric variable system. And the applicability of the forecast will be demonstrated in this part. It should be noted that all experiments in this part are based on type B aeroengines. Figures 19–21 show the details of the VSV angle prediction results. And the average value of test experiments is 2.709 (the square value of angles °). It can be seen from these figures that, compared with the forecast on the previous type of aeroengines, the prediction on this type is significantly more accurate, and the error is obviously reduced.

The same conclusion can also be obtained from the following results. Figures 22–24 show the details of the VBV angle prediction results. And the average value of test experiments is 6.973 (the square value of angles °). It should be noted that regardless of the forecasting results of VSV angles or VBV openings, the gap between the real value line and the forecasted value line is relatively low than that on the type A aeroengine. Similarly, one can see from these figures that the MAE model can track the variation of angles and openings in time.

The results in this part perform better than the results in Part 4.2.2. In other words, the forecast accuracy of type B aeroengine compressor geometric variable systems is more accurate than that of type A. While there is a little difference in data size between the two types of aeroengines,

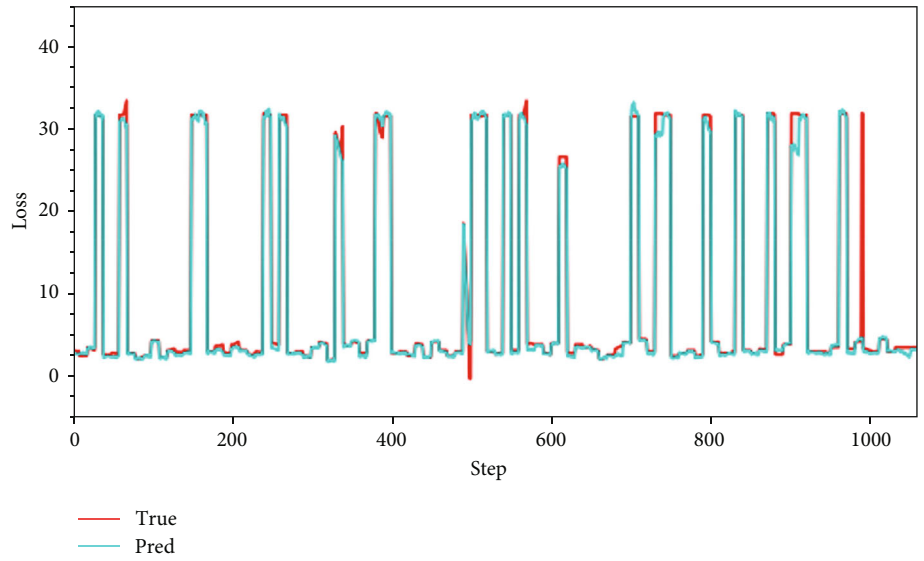

Figure 32: The steady state (VSV, type B aeroengine).

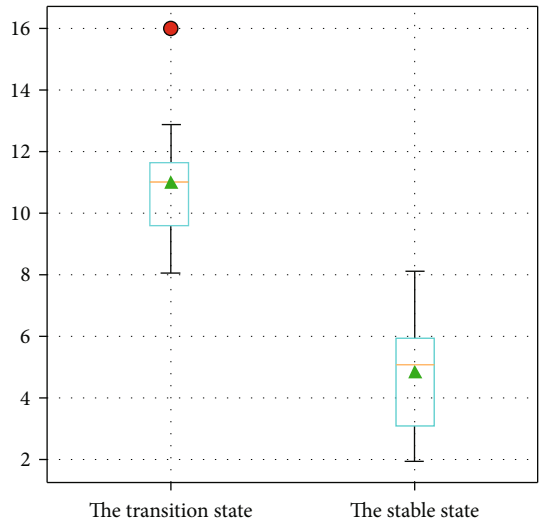

Figure 33: The box plot of the two states (VSV, type B aeroengine).

the hyperparameter set remains the same. Therefore, the reason why the results in this part are better is that the parameters we select might be more suitable for the forecast of the type B aeroengine compressor geometric variable system. And this could result in more appropriate and vital features to be learned by the MAE model. Hence, the MAE model could better analyze and track the change in the parameters that need to be forecasted. As a result, parameter selection plays an essential role in forecasting tasks. However, selecting parameters is not the main object of this article. This paper concentrates on the feasibility and applicability of forecasting the compressor geometric variable system, so the topic of parameter selection requires another subject.

4.2.3. Aeroengine State Analysis. In this part, to make our thoughts more reasonable and convincing, two groups of state experiments on VSV and VBV are carried out in this part. As mentioned above, we have performed pertinent experimental verification for the aeroengine types here. The datasets we used in this part are test datasets that have been divided into transition state and steady-state portions. It should be noted that when an airplane is in flight, the aeroengine is in its steady condition for a longer period of time than it is in its transitional state. Therefore, steady-state datasets are bigger than transition-state datasets. As can be shown that (from Figures 25–30) regardless of whether the VSV or VBV is forecast, the transition state prediction error is higher than the steady state prediction error. But the cost of forecasting the transition state of the compressor geometric variable system is still acceptable. And the MAE model can track its changes in time.

Figures 31–36 present forecasted results for the type B aeroengine. And results are similar to those above. The

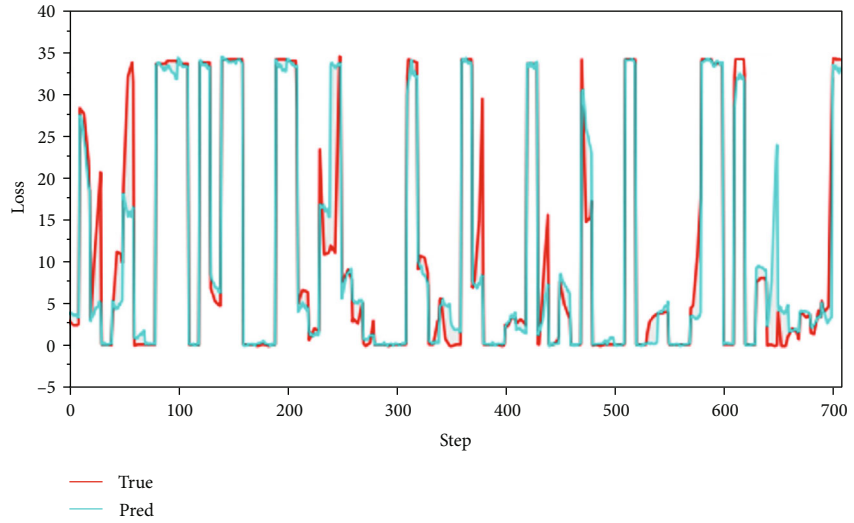

Figure 34: The transition state (VBV, type B aeroengine).

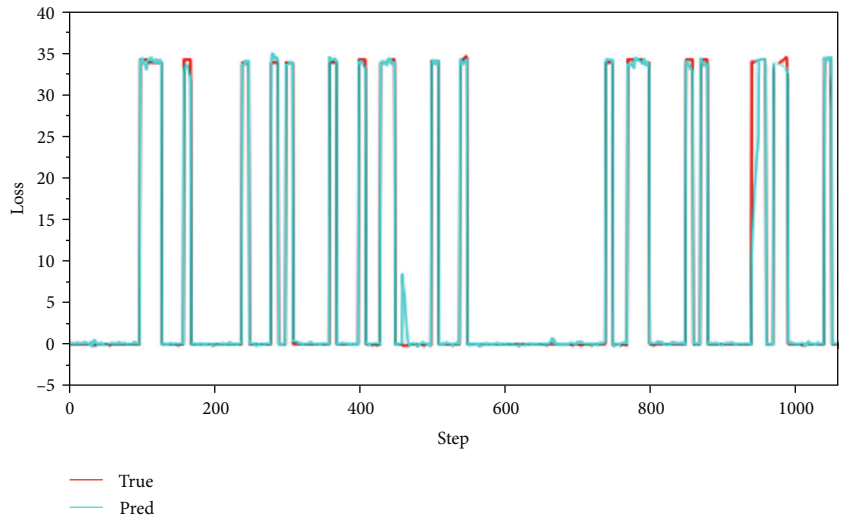

Figure 35: The steady state (VBV, type B aeroengine).

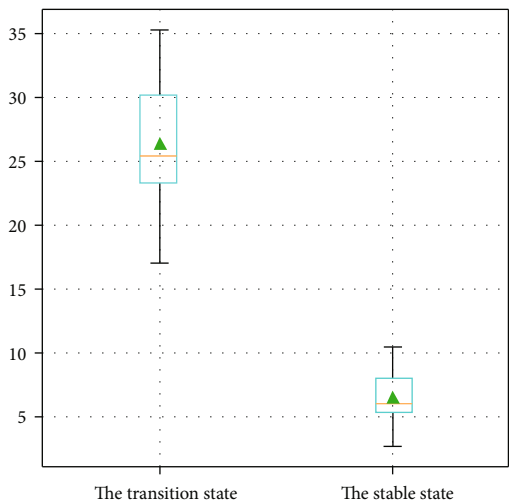

Figure 36: The box plot of the two states (VBV, type B aeroengine).

model can give relatively accurate prediction outcomes as well. This leads to an extremely crucial conclusion that even in the most complicated state, the transition state, the future trend of the system, and the quick shift in the degree may both be reliably and accurately forecasted. In addition, it is reasonable to believe that through our strategy of feeding the MAE model with randomly extracted datasets, the MAE model itself has learned the important features of distinguishing the transition state and steady state according to the input data. When the identification job is done, an accurate forecast value can be output.

5. Conclusion

This paper is aimed at studying the feasibility of predicting the compressor geometric variable system of aeroengines. We use the MAE transformer algorithm, a powerful deep learning algorithm in the AI field, and adapt it to the

aeroengine field for improvement and optimization. We predict the changes of VSV angle (°) and VBV opening (°) in the compressor geometric variable system based on the real flight dataset collected by the aircraft data acquisition system. We conduct extensive and sufficient experiments on VSV and VBV prediction to ensure the validity of our conclusions. Moreover, we test our method on different types of aeroengines and different aeroengine states to make our results more reliable and our theoretical basis more solid. Therefore, our study goes beyond the limitations of previous compressor research topics that focused on fault diagnosis, fault prognosis, and baseline modeling and demonstrates the applicability of our method on different types of aeroengines. Furthermore, the optimization and application of the MAE model in time series prediction provide an important reference for the AI field.

The study shows that (1) the forecast of the compressor geometric variable system is feasible. Both the changes in VSV angles and the changes in VBV opening can be forecasted. And it is established that both the VSV angles, and the VBV opening can be predicted with errors within an acceptable range. (2) The applicability of prediction methods specifically designed for the compressor geometric variable system was evaluated, showing relatively accurate results in different types of aeroengines. (3) Furthermore, it was verified if the model would be capable of accurately forecasting different state features when the amount of data was sufficient, thus confirming its potential to identify different aeroengine running states.

Despite the above achievements, some limitations still exist. One issue is that the system predictions do not incorporate the information of other essential parameters in the future when predicting the target values. This could lead to less accurate results if these parameters change suddenly in actual operation, even though the model may analyze their future trend. Therefore, future work will focus on collecting additional information from other crucial parameters instead of merely predicting the target values. This could provide more useful data for the model and improve its accuracy. Moreover, mechanical reasons may sometimes cause faults. Therefore, the future research direction should aim to solve these problems reasonably and efficiently.

Data Availability

The datasets we used were collected from airlines. And the companies must approve the usage rights. Due to the confidentiality of our datasets, authorization must also be obtained before uploading them. Therefore, after contacting the company and obtaining permission, we will upload the data.

Disclosure

Our previous project included the paper (https://ieeexplore.ieee.org/document/9910038) [28]. The author is also the same. There was overlap because the former's datasets and data processing techniques are close to those in this article. The most important research topics and directions, however, differ. The purpose of this work is to advance the forecasting research of additional key aeroengine systems (the compressor geometric variable system) based on the results of our past research.

Conflicts of Interest

The authors declare that they have no conflicts of interest.

Authors' Contributions

Cunjiang Xia and Yuyou Zhan contributed equally to this work.

Acknowledgments

This work was supported by the Key R & D plan of Sichuan Provincial Department of Science and Technology (grant number 2022YFG0356), the Key R & D plan of Tibet Science and Technology Department (grant number XZ202101ZY0017G), the Civil Aviation Administration of China education and training program (grant number 0252001), and the Fundamental Research Funds for the Central Universities (grant number J2022-014).

References

[1] J. Lee and H. Wang, "New technologies for maintenance," in *Complex System Maintenance Handbook*, pp. 49–78, Springer, London, 2008.

[2] M. Xiong, H. Wang, Q. Fu, and Y. Xu, "Digital twin–driven aero-engine intelligent predictive maintenance," *The International Journal of Advanced Manufacturing Technology*, vol. 114, no. 11-12, pp. 3751–3761, 2021.

[3] S. Liu, B. Yan, T. Zhang, X. Zhang, and J. Yan, "Three-dimensional coverage-based cooperative guidance law with overload constraints to intercept a hypersonic vehicle," *Aerospace Science and Technology*, vol. 130, article 107908, 2022.

[4] S. Liu, B. Yan, T. Zhang, P. Dai, R. Liu, and J. Yan, "Three-dimensional cooperative guidance law for intercepting hypersonic targets," *Aerospace Science and Technology*, vol. 129, article 107815, 2022.

[5] S. Liu, B. Yan, T. Zhang, X. Zhang, and J. Yan, "Coverage-based cooperative guidance law for intercepting hypersonic vehicles with overload constraint," *Aerospace Science and Technology*, vol. 126, article 107651, 2022.

[6] E. M. Greitzer, "Axial compressor stall phenomena," *Journal of Fluids Engineering*, vol. 102, no. 2, pp. 134–151, 1980.

[7] F. Willems and B. De Jager, "Modeling and control of compressor flow instabilities," *IEEE Control Systems Magazine*, vol. 19, no. 5, pp. 8–18, 1999.

[8] A. J. Volponi, "Gas turbine engine health management: past, present, and future trends," *Journal of Engineering for Gas Turbines and Power*, vol. 136, p. 5, 2014.

[9] H. M. Castilho, C. L. Nascimento, and W. O. L. Vianna, "Aircraft bleed valve fault classification using support vector machines and classification trees," in *2018 Annual IEEE International Systems Conference (SysCon)*, Vancouver, BC, Canada, 2018.

[10] B. Li, C. Gu, X. Li, and T. Liu, "Numerical optimization for stator vane settings of multi-stage compressors based on neural

networks and genetic algorithms," *Aerospace Science and Technology*, vol. 52, pp. 81–94, 2016.

[11] Y. Tan, "Fitting operation curve of civil aviation turbo-fan engine's variable bleed valve based on MATLAB," *Journal of Physics: Conference Series*, vol. 1176, no. 5, 2019.

[12] L. Wang, L. Zhang, M. Xu, and X. Shi, "Research on fault diagnosis method of civil aviation engine variable bleed valve system based on artificial immune algorithm," *International Journal of Pattern Recognition and Artificial Intelligence*, vol. 30, no. 7, article 1659021, 2016.

[13] C. Huiling, L. Lixiao, and Q. Chungang, "Study of the surge fault diagnosis of an aeroengine based on the LS-SVM(least square-supporting vector machine)," *Journal of Engineering for Thermal Energy and Power*, vol. 28, no. 1, pp. 23–27, 2013.

[14] F. Xuyun, S. Zhenyong, and L. Zhen, "Time-varying fuzzy neural network and its application in prediction of exhaust gas temperature," *Computer Integrated Manufacturing System*, vol. 20, no. 4, pp. 919–925, 2014.

[15] L. Shuming, R. Pei, and H. Yanxiao, "Fitting of aero engine baseline equation," *Mechanical Engineering and Automation*, vol. 1, pp. 153-154, 2016.

[16] J. Xu and X. Lei, "Health management based on fusion prognostics for avionics systems," *Journal of Systems Engineering and Electronics*, vol. 22, no. 3, pp. 428–436, 2011.

[17] C. F. M. I. Customer Training Center, *Training manual CFM56-7B engine systems*, CFMI, 2012.

[18] CFM company, *CFM56-7B Advanced Engine System*, GE Customer training center, Cincinnati, 2016.

[19] N. A. Jalil, H. J. Hwang, and N. M. Dawi, "Machines learning trends, perspectives and prospects in education sector," in *Proceedings of the 2019 3rd International Conference on Education and Multimedia Technology*, New York, 2019.

[20] T. Mitchell, *Key Ideas in Machine Learning*, Carnegie Mellon University, 2017.

[21] K. He, X. Chen, S. Xie, Y. Li, P. Dollár, and R. Girshick, "Masked autoencoders are scalable vision learners," 2021, http://arxiv.org/abs/2111.06377.

[22] A. Vaswani, N. Shazeer, N. Parmar et al., "Attention is all you need," *Advances in Neural Information Processing Systems*, vol. 30, 2017.

[23] J. Devlin, M. W. Chang, K. Lee, and K. Toutanova, "Bert: pre-training of deep bidirectional transformers for language understanding," 2018, http://arxiv.org/abs/1810.04805.

[24] K. He and J. Sun, "Convolutional neural networks at constrained time cost," in *Proceedings of the IEEE conference on computer vision and pattern recognition*, Boston, USA, 2015.

[25] R. K. Srivastava, K. Greff, and J. Schmidhuber, "Highway networks," 2015, http://arxiv.org/abs/1505.00387.

[26] I. Loshchilov and F. Hutter, "Decoupled weight decay regularization," 2017, http://arxiv.org/abs/1711.05101.

[27] J. Hu, L. Shen, and G. Sun, "Squeeze-and-excitation networks," in *Proceedings of the IEEE conference on computer vision and pattern recognition*, pp. 7132–7141, Salt Lake City, 2018.

[28] C. Xia, Y. Zhan, Y. Tan, and W. Wu, "Research on forecasting aeroengine vibration signals based on the MAE model," *IEEE Access*, vol. 10, pp. 110676–110688, 2022.